Liu, Enbin; Ma, Xi; Zhou, Mo

**Article**

# Analysis of discharge process of oil pipeline with complex topography

Energy Reports

**Provided in Cooperation with:**
Elsevier

*Suggested Citation:* Liu, Enbin; Ma, Xi; Zhou, Mo (2019) : Analysis of discharge process of oil pipeline with complex topography, Energy Reports, ISSN 2352-4847, Elsevier, Amsterdam, Vol. 5, pp. 678-687,
https://doi.org/10.1016/j.egyr.2019.06.008

This Version is available at:
https://hdl.handle.net/10419/243621

Energy Reports 5 (2019) 678–687

Contents lists available at ScienceDirect

Energy Reports

journal homepage: www.elsevier.com/locate/egyr

Research paper

# Analysis of discharge process of oil pipeline with complex topography

Enbin Liu *, Xi Ma, Mo Zhou

*Southwest Petroleum University, Chengdu 610500, China*

ARTICLE INFO

*Article history:*
Received 4 February 2019
Received in revised form 15 May 2019
Accepted 19 June 2019
Available online xxxx

*Keywords:*
Big drop
Oil pipeline
U-type
Water discharge
Leaking aperture

ABSTRACT

During the commissioning process of "first injection of crude oil after water injection", due to the density difference between crude oil and water, the oil pressure on the left side of the "U" section is less than the right hydraulic pressure, and the running process of the oil head is stagnated in a hilly oil pipeline with high elevation difference. Concerning this problem, solution of discharging pressure by using relief valve in valve station nearby oil–water interfacial point is proposed in this paper. According to the actual data, gas–liquid flow in a gas-cap empty process of a big drop and hilly oil pipeline was numerically investigated by dynamic multiphase simulation software OLGA. Simulation data in terms of flow rate, pressure and leakage were compared under different leaking apertures. The simulation results show that the general pressure variation tendencies at the vent, bottom point or top and low elbows show no connection with vent diameters but its final fluctuation that the smaller the diameter is, the more intensive the fluctuation gets.. And as for the emptying of a big drop and hilly pipeline, appropriate increase of leaking aperture can improve the drainage ratio (leakage/general capacity of the pipeline) and drainage rate, but excessive aperture will cause severe negative pressure and breakage cavity which foster the likelihood of close water-surge and damage to the pipe safety.



## 1. Introduction

The drainage process of a big drop pipe is actually a two phase flow process. Under the inlet and outlet (vent point) backpressure, a two-phase flow is formed at the beginning of leakage (Laanearu et al., 2012; Tijsseling et al., 2016). Due to the deformable interface, the existence of compressible gas phase and the three-dimensionality of tube flow, gas–liquid two-phase flow is the most complicated of the two-phase flow (Ishii and Mishima, 1984; Taitel et al., 1995). In the actual situation of pipeline operation, the parameters of different positions in the pipe are difficult to achieve stability. For some pipes, however, the variation of process parameters is small especially when operating under steady condition (El-Oun, 1990), which belongs to slow transient flow. Therefore, it is also acceptable to use steady models to approximately describe normal conditions of pipelines and calculate the distribution of processing parameters. Taitel et al. (1995) aimed at slow transient flow based on the assumption that the gas in gas–liquid flow is under quasi-steady state, a four-equation model are established which is characterized by dynamic liquid phase continuity equation and three models of steady state equation. This simplified model can be applied to all kinds of flow patterns and obtain stable numerical solutions, but it cannot deal with complex flow problems and the result is not accurate enough.

In order to accurately simulate the change of pipe flow, transient flow model should be used for analysis. Because of the three-dimensional characteristics of gas–liquid two-phase flow and the large flow rate in long distance pipe flow, it is impractical to use the three-dimensional model based on Navier–Stokes equations to study transient two-phase flow (Liu et al., 2019a,b; Yacin et al., 2010). For these reasons, one-dimensional two-phase flow models have been extensively employed over the past decades. The most popular two-phase flow models currently in use are the two-fluid models, which are based on one-dimensional balance equations of mass, momentum and energy for each phase (Ishii and Mishima, 1984). Since considering friction between gas and liquid as well as effects of momentum transfer on the flow process, Eulerian-Eulerian models are capable of reflecting subtle characteristics of two fluids both in gas–liquid flow and suitable to describe intensive motions on free surface and mobility capture of interfaces between phases (e.g. in Yeoh and Tu (2010), Pouraria et al. (2017), Mohammadzaheri et al. (2019) and Guo et al. (2014)).

If we categorize these two-fluid models developed during the past 20 years by classes based on the number of equations contained, the simplest shall be single-pressure four-equation models, such as the ones used by Masella et al. (1998), Omgba-Essama (2004), Bonizzi and Issa (2003) and Issa and Kempf (2003), consists of two mass and momentum equations and ignoring the unevenness of pressure distribution throughout the cross-section area. In terms of flow patterns without apparent phase-interface

* Corresponding author.
*E-mail address:* enbin.liu@swpu.edu.cn (E. Liu).

https://doi.org/10.1016/j.egyr.2019.06.008

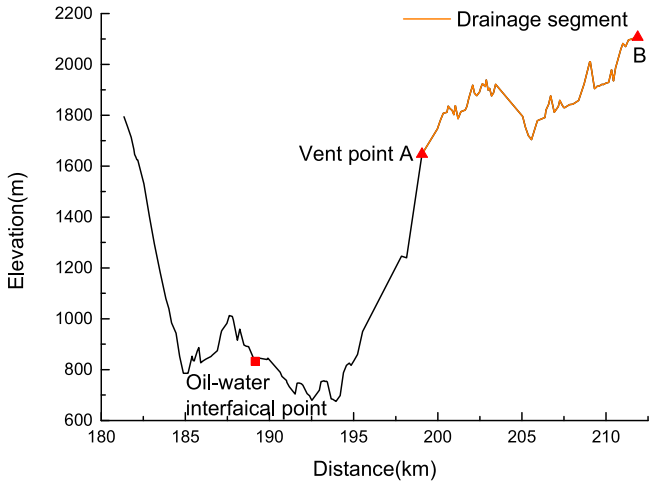


**Fig. 1.** Nujiang crossing pipes.

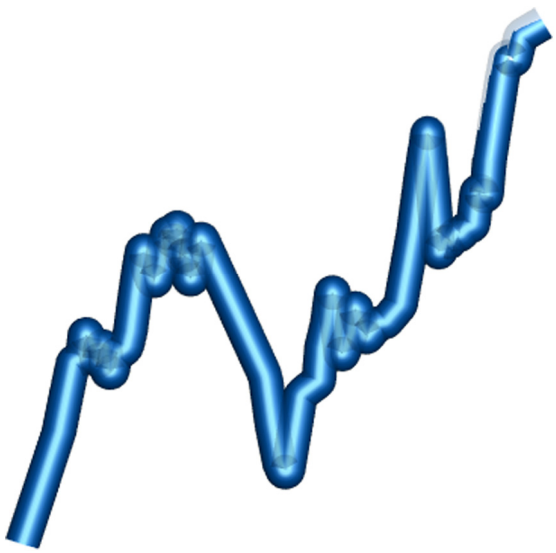

**Fig. 2.** 3D diagram of emptying segment AB.

curvature effects, the four-equation model is sufficient. Nevertheless, pressure difference between phases throughout pipe cross section may become nonegligible when curvature effects are significant, thus it is inevitable to turn to two-pressure models. Based on the previous four-equation model, Loilier et al. (2005) proposed a five-equation two-fluid model with an extra energy equation for the mixture as a whole by considering the evolution of volume fraction, which overlooked the temperature differences between components and taking energy transfer into account. More integrated two-fluid models with six equations, using mass, momentum, energy equations of gas and liquid, were introduced by Ishii and Mishima (1984) and Simões et al. (2014). Besides of these, Saurel and Abgrall (1999) presented a seven-equation two-fluid model by add an equation for the volume-fraction evolution and came up with a simple HLLC-type Riemann solver to calculate impedance of flow patterns, velocities and pressures on the phase interfaces with his co-workers, Métayer et al. (2007) and Furfaro and Saurel (2015). In addition, there are even more complex two-pressure seven-equation two-fluid models as used in Emonot et al. (2011), Slolan et al. (1992) and Chao et al. (2016).

Despite single-pressure models are the simplest among all available two-fluid models, the forms of equations in the model changes with the development of flow regime and transient response in pipeline systems is relatively slow, it is not that the more complex the model, the better, but the choice of the specific physical conditions (e.g. in Liu et al. (2019a,b), Shanfang et al. (2013) and Seung et al. (2017)). As Masella (1998) put it in his comparative study, simpler forms of transport equations, matched with less time-consuming numerical algorithms, may be good enough to simulate oil-gas two-phase flow.

Abnormal conditions and accidents occurred during commissioning of long-distance pipelines located in hilly and big drop areas are complicated and diverse. Hence, causes and solutions of these abnormal conditions are various according to different engineering realties and the existing researches for the sake of solving problems raising in the production cannot settle every situation (Hongfang et al., 2019).

## 2. Problem description

Nujiang crossover pipes, located in hilly and rugged areas, contain big drop U-type segments of which the maximum relative height difference reaches 1432.64 m as shown in Fig. 1.

In the commissioning process of "first injection of crude oil after water injection", due to the density difference between crude oil and water, the oil pressure on the left side of the "U" section is less than the right hydraulic pressure, and the running process of the oil head is stagnated. This will not only delay the commissioning of the pipeline, but also lead to a great increase in the amount of mixed oil and the load of sewage process at the final station.

Concerning these, solution of pipe pressure discharge by using relief valve in valve station (A) nearby the oil–water interfacial point is put forward in this paper: the emptying pipeline segment starts from valve station A and ends at valve station B (as shown in Figs. 1 and 2). As shown in Fig. 2, the featured segment is not completely full with water, there is air gathering at the peak of the end (B). This is because in order to ensure commissioning safety and avoid security risks because of the direct contact between air and oil, a progress of water isolation was conducted. One thing needs to be declared that the pipeline is full of air before water injection. When the running process of the oil head is stagnated the water isolation did not completely squeeze the air out of the pipeline, as a result, there is gas gathering at the peak of the end (B). As the consequence of big drop and many peak and valley elbows, water flows out from station A under the gravity and pressure and there must be water remained at the low elbows (as shown in Fig. 3). Since the pressure in the pipeline continues to drop with emptying which arouses a great chance of negative pressure at the peak elbows—the pressure at the peak less than or equal to the saturated vapor pressure of water causing water vaporization and cavitation (as shown in Fig. 4), the discharging process is a gas–liquid two-fluid flow.

When a hilly oil and gas pipeline with high elevation difference studied, it is important to consider the potential hazards of hydrate (e.g. in Liu et al. (2017), Lu et al. (2017)). However the studied fluid in this paper is water and there is no any natural gas but air in the pipe as described in last paragraph. And the ambient temperature is about 295 K, as a result, the simulation of hydrate forming is not conducted.

To ensure the pressure of the oil column overcoming the pressure of the water column and the height difference between them, it is necessary to remove the water from the pipe as much as possible. Inspired by the gas-cap emptying study in the mobile pipeline of Guo et al. (2017), which shows that the OLGA numerical simulation results are in good agreement with experiment results, the steady and transient conditions of drainage

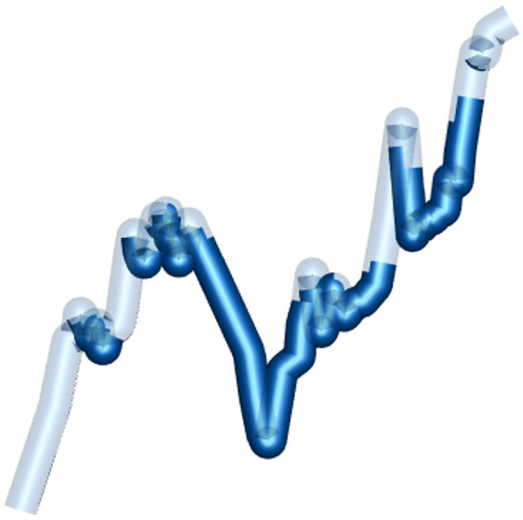

**Fig. 3.** Water remained at the valley elbows.

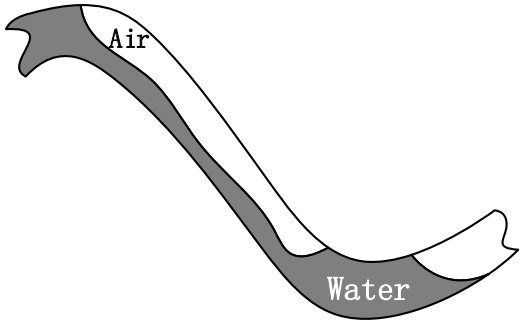


**Fig. 4.** Air gathering at the peak.

process in this hilly oil pipeline was investigated numerically by OLGA7.0, based on actual geometric and geographic data of Nujiang crossing pipes. After enormous calculations, simulation results including a set of available leaking apertures, the minimum discharge time, the maximum leakage and optimal leaking aperture range of the target pipe segments were obtained and applied to engineering situation which acquired good effects.

## 3. Physical and numerical models

### 3.1. Physical models

The simulation of drainage process in commissioning is featured with a big drop and hilly section on the right side of the giant U-type pipe (see Fig. 1).

As shown in Fig. 5, the discharged pipe segment is typical hilly which contains at least five rugged sections with elevation difference more than 100 meters and has the only one vent point.

The simulation diameter of pipeline is 813 mm according to the actual situation. The total length of pipeline is 13034.5 m and the pipeline is laid in a buried way. Since the height difference between the inlet and outlet of the pipeline is about 500 m, there is no need to use air compressor at the inlet and the outlet (vent point) is directly connected with atmosphere. Simulation flowchart (a) and node definition (b) are shown in Fig. 6.

The design parameters and initial boundary conditions of the target pipeline are listed in Tables 1 and 2, respectively.

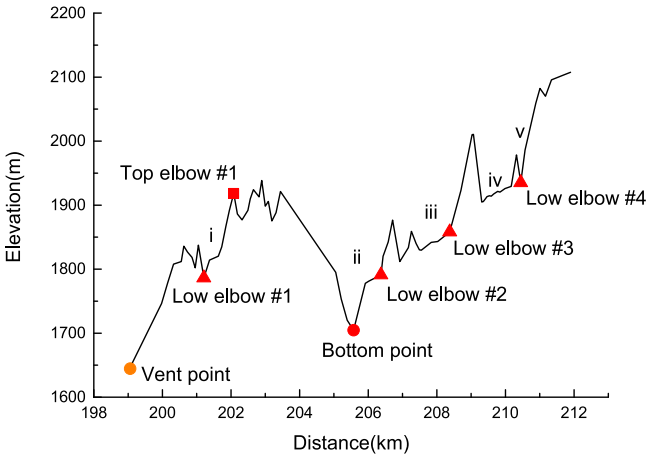


**Fig. 5.** Geography of the featured drainage section.

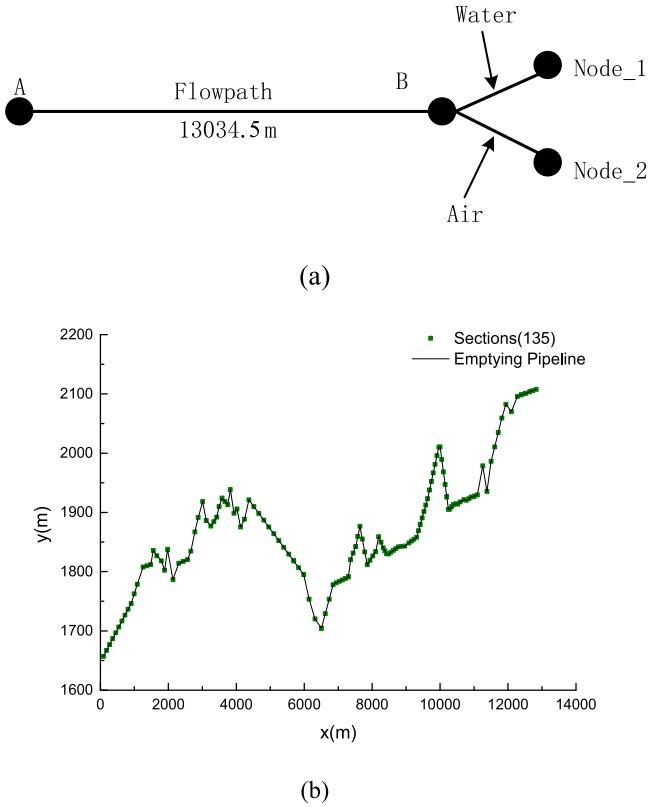


**Fig. 6.** Simulation flowchart (a) and node definition (b).

**Table 1**
Design parameters of target drained pipe segment.

| Design pressure (MPa) | Wall thickness (mm) | Diameter (mm) | Roughness (mm) |
|---|---|---|---|
| 15 | 17.5 | 813 | 0.04 |

The valve maneuvering time in Table 2 is determined by $t_0 = \frac{2l}{\sqrt{\frac{E}{\rho\left(1+\frac{Ed}{E_0\delta}\right)}}} = 13.3$ s, where $l$ is pipeline length, $E$ is volume modulus of water, $E_0$ is volume modulus of pipe, $\delta$ is wall thickness, $d$ is diameter of pipeline, $\rho$ is density of water, $t_0$ is the valve maneuvering time to avoid direct water hammer.

**Table 2**
Initial boundary conditions.

| Inlet massflow (kg/h) | Back pressure at the vent (MPa) | Inlet and outlet temperature (K) | Outlet pressure (MPa) |
|---|---|---|---|
| 900 | 0.1 | 295 | 0.1 |
| Check valve | | | |
| Valve maneuvering time | | Valve type | Type of valve opening |
| ≥13.3 s | | Ball valve | Lineal |

Conversion between liquid valve sizing coefficient ($C_v$) and orifice area in OLGA are determined as following OLGA (2014):

The orifice equation for an incompressible fluid is:

$$\Delta P_{Orifice} = \frac{1}{2}\left[\left(\frac{A}{A_{Orifice} \bullet C_d}\right)^2 - 1\right] \bullet W_{Total} \bullet \sum_i \alpha_i \bullet u_i = \frac{1}{2}\left[\left(\frac{A}{A_{Orifice} \bullet C_d}\right)^2 - 1\right] \bullet \left(\frac{Q}{A}\right)^2 \bullet \rho_{Fluid} \quad (1)$$

In Eq. (1), $\rho_{Fluid}$ is the fluid density, $Q$ is the volumetric flow rate, $\alpha_i$ is volumetric fraction of mass field i, $u_i$ is velocity of mass field I, A is pipeline area, $A_{Orifice}$ is orifice area, $C_d$ is orifice discharge coefficient, $\Delta P_{Orifice}$ is orifice pressure drop.

The valve sizing equation is:

$$Q = C_v \bullet \sqrt{\frac{\Delta P_{Sizing}}{g}} = C_v \sqrt{\frac{\Delta P_{Sizing} \bullet \rho_{Red}}{\rho_{Fluid}}} \quad (2)$$

In Eq. (2), $C_v$ is valve sizing coefficient, $Q$ is the volumetric flow rate, $\Delta P_{Sizing}$ is sizing pressure drop, $\rho_{Red}$ is water density at 4° C and 1 atmosphere (998.840 kg/m$^3$), $\rho_{Fluid}$ is fluid density at reference conditions.

Setting $\Delta P_{Orifice} = \Delta P_{Sizing}$ and solving for $C_v$ or orifice area ($A_{Orifice}$) is:

$$C_v = \frac{A}{\sqrt{\frac{\rho_{Red}}{2} \bullet \left[\left(\frac{A}{A_{Orifice} \bullet C_d}\right)^2 - 1\right]}} \Leftrightarrow A_{Orifice} = \frac{A}{C_d \sqrt{\frac{2A^2}{C_v^2 \bullet \rho_{Red}} + 1}} \quad (3)$$

Above it is assumed that the orifice equation is given with same units as the sizing equation.

In addition to the parameters shown in Tables 1 and 2, other values in OLGA, like ambient temperature, heat transfer coefficient etc. are all kept default. Fluid files including physical properties of gas and liquid are generated by PVT simulation software PVTsim by setting the gas to air and the liquid is set to water.

### 3.2. Numerical models

Since the featured pipeline is buried without insulating layer and the ambient temperature difference along the pipeline is minor as well as the studied fluid is water which is not sensitive to temperature, to simplify calculation, thermodynamic process is not considered and it is assumed that the two-phase flow in pipelines is one-dimensional and isothermal in calculated cells, the microscopic properties of phases and uneven distribution of pressures at cross section of the pipe are negligible, namely regard the pressure as uniformed. It is also hypothesized that tensions on interfaces between phases and phase/wall and stresses raised by turbulent fluctuation can be leaved out. In OLGA, flow regime is considered as an essential part of two-phase flow model

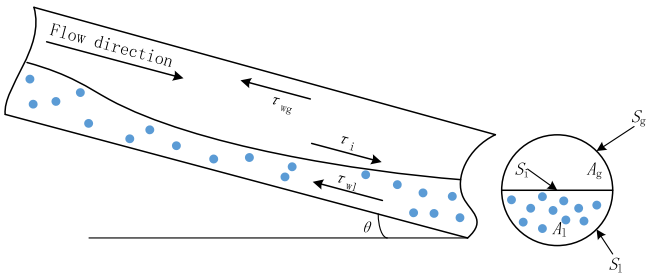


**Fig. 7.** Schemata of gas-liquid flow.

in which the liquid phase exists as liquid droplets at the wall or in the gas nucleon.

Based on the analysis above and the physical models, a single-pressure six-equation two-fluid model is derived by applying three separate continuity equations for gas, liquid bulk and liquid droplets, which may be coupled through interfacial mass transfer, two momentum equations and a mixture energy-conservation equation. By selecting a micro unit, as Fig. 7, an improved OLGA two fluid model can be deduced according to the laws of conservation (e.g. in OLGA (2014), Liu et al. (2019a,b) and Liu et al. (2016)):

***Mass Transport Equations***

For the gas phase (e.g. in Shanbi et al. (2018)),

$$\frac{\partial}{\partial t}\left(\beta_g \rho_g\right) = -\frac{1}{A}\frac{\partial}{\partial x}\left(A\beta_g \rho_g u_g\right) + \Psi_g + q_g \quad (4)$$

For the liquid phase at the wall,

$$\frac{\partial}{\partial t}\left(\beta_l \rho_l\right) = -\frac{1}{A}\frac{\partial}{\partial x}\left(A\beta_l \rho_l u_l\right) - \Psi_g \frac{\beta_l}{\beta_l + \beta_d} - \Psi_e + \Psi_d + q_l \quad (5)$$

For liquid droplets,

$$\frac{\partial}{\partial t}\left(\beta_l \rho_l\right) = -\frac{1}{A}\frac{\partial}{\partial x}\left(A\beta_d \rho_l u_d\right) - \Psi_g \frac{\beta_d}{\beta_l + \beta_d} - \Psi_e + \Psi_d + q_d \quad (6)$$

In Eqs. (4)–(5), $u_g = R_D(u_l + u_r)$ where $R_D$ is slip ratio and determined by flow regime, $R_D = 1$ when separated flow.

***Momentum balance equations***

A combined equation for the gas and possible liquid droplets is

$$\begin{aligned}\frac{\partial}{\partial t}\left(\beta_g \rho_g u_g + \beta_d \rho_l u_d\right) &= -\left(\beta_g + \beta_d\right)\frac{\partial p}{\partial x} \\ &-\frac{1}{A}\frac{\partial}{\partial x}\left(A\beta_g \rho_g u_g^2 + A\beta_d \rho_l u_d^2\right) - \frac{\Gamma_{gw}}{A} - \frac{\Gamma_i}{A} \\ &-\left(\beta_g \rho_g + \beta_d \rho_l\right) g \sin\theta + \Psi_g \frac{\beta_l}{\beta_l + \beta_d} u_a + \Psi_e u_i - \Psi_d u_d\end{aligned} \quad (7)$$

where $\frac{\Gamma_{gw}}{A} = \frac{\tau_{wg} S}{H}$, $\frac{\Gamma_i}{A} = \frac{\tau_i S}{H}$.

For the liquid at the wall,

$$\begin{aligned}\frac{\partial}{\partial t}\left(\beta_l \rho_l u_l\right) &= -\beta_l \frac{\partial p}{\partial x} - \frac{1}{A}\frac{\partial}{\partial x}\left(A\beta_l \rho_l u_l^2\right) - \frac{\Gamma_{lw}}{A} + \frac{\Gamma_i}{A} \\ &- \beta_l \rho_l g \sin\theta + \Psi_g \frac{\beta_l}{\beta_l + \beta_d} u_a - \Psi_e u_i + \Psi_d u_d \\ &- \beta_l D\left(\rho_l - \rho_g\right) g \frac{\partial \beta_l}{\partial x} \cos\theta\end{aligned} \quad (8)$$

where $\frac{\Gamma_{lw}}{A} = \frac{\tau_{wl} S}{H}$.

In Eqs. (7)–(8), $u_a$ is the velocity of phase changing section including evaporation from liquid film and liquid droplets when vaporing happens; $u_{0d}$ is the falling velocity of droplets and

$$u_{0d} = \left[\frac{4 g d_d \left(\rho_l - \rho_g\right)}{3 C_d \rho_g}\right]^{0.5} \quad (9)$$

**Table 3**
Value of coefficient $C_d$

| Flow regime | $R_e$ | $C_d$ |
|---|---|---|
| Laminar flow | $R_e \leq 2$ | $24R_e^{-1}$ |
| Transition flow | $2 < R_e \leq 500$ | $18.5R_e^{-0.6}$ |
| Turbulent low | $500 < R_e \leq 2 \times 10^5$ | 0.44 |
| | $R_e > 2 \times 10^5$ | 0.1 |

**Table 4**
Leaking apertures and relevant leakages.

| Leaking aperture (mm) | Maximum leakage ($m^3$) | Simulation end time (h) | Settling time of flow rate at the vent (h) |
|---|---|---|---|
| 30 | 2950 | 72 | 56.16 |
| 50 | 3256 | 72 | 53.07 |
| 70 | 3260 | 72 | 48.6 |
| 90 | 3342 | 72 | 19.44 |
| 100 | 3375 | 72 | 18.05 |
| 110 | 3320 | 72 | 20.83 |
| 130 | 3252 | 72 | 21.66 |
| 168 | 3239 | 72 | 23.22 |
| 200 | 3323 | 72 | 24.05 |

In Eq. (9), $C_d$ is the settling resistance coefficient of droplets and determined by Reynolds number$R_e$, as shown in Table 3:

***Energy Equation***

Because of the hypothesis of equivalent temperatures of gas and liquid, and the energy balance equation can be written as

$$\frac{\partial}{\partial t}\left[\rho_g A\phi_g dx\left(E_g+\frac{1}{2}u_g^2+gh\right)+\rho_l A\phi_l dx\left(E_l+\frac{1}{2}u_l^2+gh\right)+\rho_l A\phi_d dx\left(E_d+\frac{1}{2}u_d^2+gh\right)\right]dt = -\frac{\partial}{\partial x}\left[G_g\phi_g dt\left(h_g+\frac{1}{2}u_g^2+gh\right)+G_d\phi_d dt\left(h_d+\frac{1}{2}u_d^2+gh\right)+G_l\phi_l dt\left(h_l+\frac{1}{2}u_l^2+gh\right)\right]dx+Hs+U \quad (10)$$

In Eq. (10), $G$ represents mass flow and $G_g = \rho_g u_g A$, $G_l = \rho_l u_l A$, $G_d = \rho_l u_d A$.

### 3.3. Numerical methods

On the basis of the two-fluid model, OLGA uses staggered grid method and the finite volume method (FVM) to discretize the pipeline into control units while the parameters of the pipeline, such as density, pressure and temperature, are stored in the center of the control unit and other variables (velocity and flux) are calculated at the boundary. Then OLGA employs Euler scheme combined with Lagrangian front-tracking format method to solve the basic equations in the model.

## 4. Results and discussions

### 4.1. Leaking apertures and leakage

After simulation calculations, a set of available leaking apertures (30 mm–200 mm) and the relevant leakage are obtained, as shown in Table 4, by taking the vent diameter as independent variable. Simulation end time is set to 72 h to make sure of a complete discharge. Since the same end time and capacity of the pipeline, the maximum leakage shown in Table 4 could reflect the discharge rates of different leaking apertures directly.

As shown in Fig. 8, when the leaking aperture augments, the settling time of flow rate at the vent decreases first and then climbs a little bit. Among them, the settling time of the minimum leaking aperture 30 mm is the longest, which is 56.16 h; the shortest settling time is leaking aperture 100 mm, 18.05 h. Table 4 indicates that the computing time of data is long enough while the difference value of maximum leakages among different apertures is minor. When the leaking aperture ranges from 30 mm∼200 mm, the maximum leakage ranges from 3239 $m^3$∼3375 $m^3$.

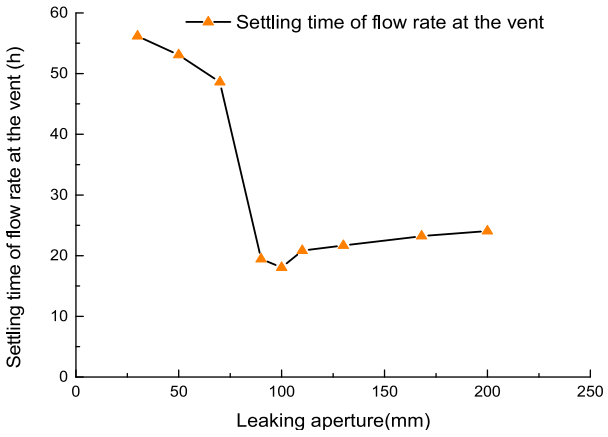


**Fig. 8.** Settling time of flow rate at the vent-leaking aperture relation curve.

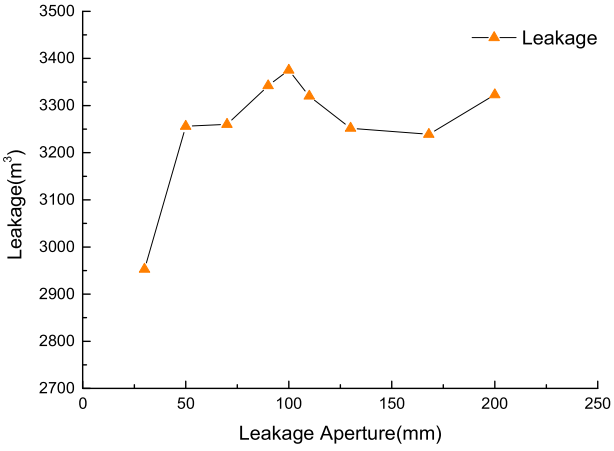


**Fig. 9.** Leaking aperture-leakage relation curve.

Liquid hold up in pipe-time relation curves of different leaking apertures is shown in Fig. 9.

Fig. 9 shows that the displacement of maximum leakages of different apertures is not much. Since the same simulation end time and capacity of the discharged pipeline, Fig. 9 could reflect the drainage ratio (maximum leakage/capacity of the pipeline) of different leaking apertures directly. As shown in Fig. 9, when aperture is greater than 90 mm, the drainage ratio is higher than that of the leaking aperture less than 90 mm. It is because that a big drop and hilly pipe full of water will form the hydrops in elbow place during the drainage, with the increase of leaking aperture, drainage rate accelerated, drainage process becomes more fierce, the residual kinetic energy of the hydrops increases, the greater the residual kinetic energy gets, the easier water effuses out of the elbow, so as to make the leakage increases, but the interval of reaching stability state of hydrops also increases with the increase of displacement speed, so the leakage in the same drainage time is different.

Fig. 10 shows the drainage time of the same leakage (2100 $m^3$) for each leak aperture, and the drainage rate under each leaking

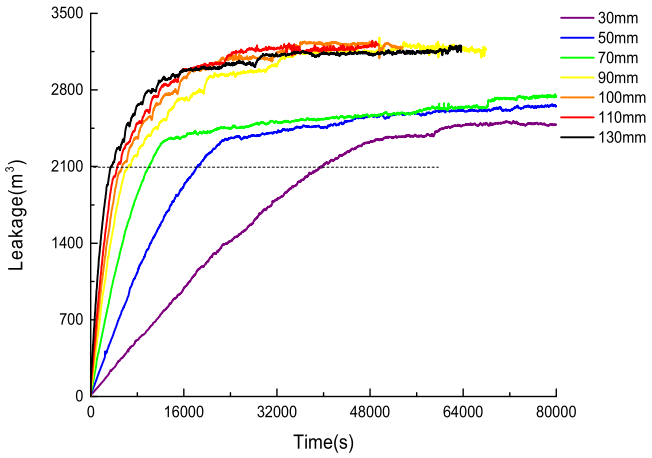


**Fig. 10.** Leakage-time relation curves.

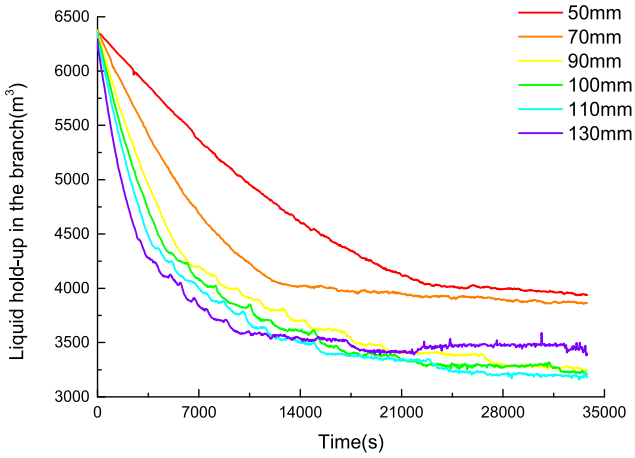


**Fig. 11.** Liquid hold-up in pipeline-time relation curves.

aperture can be seen directly. Obviously, the smaller the leaking aperture is, the slower the drainage rate will be. When the aperture is 130 mm, the required drainage time is the shortest (6583 s ≈ 1.8 h). When the aperture is 30 mm, the required drainage time is the longest (65 924 s ≈ 18.31 h), which is about 10 times of the minimum drainage time, and the drainage rate is too slow, therefore, this condition is not considered in the following sections (leaking aperture D = 30 mm). Due to the engineering practice, it is inadvisable to trepanning the oil pipeline directly, but portiforium on the branch pipe of relief valve chamber is acceptable. When the main pipe diameter of the valve chamber is ∅ 813, the biggest allowable diameter of its branch pipe is 168.3 mm, so the scope of the leak aperture is narrowed to 50 mm∼130 mm. Thus the drainage process of leaking aperture of 50 mm∼130 mm will be emphatically analyzed below.

As demonstrated in Fig. 11, the drainage process gets more intensive and rapid as the leaking aperture increases; liquid hold-up in the pipeline reduces quickly first and then extremely slowly. Because with the leaking aperture increasing, the drainage process is accelerated, and the faster the discharge is, the easier it is to enter the low-elbow water agitation stage (the hydrops effused from the low elbow due to the inertance). Since the residual kinetic energy of hydrops in low elbow increases with the acceleration of drainage, the greater the residual kinetic energy is, the more effusion from the low elbow will be, hence leading to less liquid hold-up in the pipeline. However, as it is a big drop and rugged pipeline, there are too many low elbows, which takes a long time for the effused water from the upstream low elbows to reach the vent point. So when the drainage is carried out for a certain period of time, the amount of holding liquid drops very slowly in the float.

### *4.2. Engineering drainage end time and settling time of flow rate at the vent*

#### *4.2.1. Engineering drainage end time*

The purpose of this article is to obtain the best leaking aperture and the corresponding drainage time applicable to the actual engineering situation, but the drainage end time for actual engineering situation and the drainage end time for theoretically complete drainage are two different concepts, the pipeline in the actual engineering in fact does not need to be completely drained (i.e., there is no longer any water flowing through the vent point). As shown in Fig. 8, after a rapid decline, the liquid volume of drain pipeline decreases at an extremely slow speed, which should be a constant value for the theoretical completely emptying phase. Apparently the required time for theoretically complete drainage is far beyond the reasonable range for a discharge operation in engineering practice. Consequently the engineering drainage end time should not be the theoretically complete drainage end time.

Based on this, flow monitoring point is set at the vent to observe the flow changes of the vent so as to estimate the progress of the drainage, engineering drainage end time will be the settling time of flow rate at the vent

#### *4.2.2. Settling time of flow rate at the vent*

In Fig. 8, liquid hold-up in the pipe decreases over time. From the beginning of drainage to a certain timing, which the bigger the vent diameter is, the closer the timing is to start point, there is a significant reduction of the liquid hold up and the drainage process is quite efficient during this period. After that certain point in time, liquid hold up decreases at an extremely slow speed and takes a long time to become a constant value. Consequently, it is not accurate enough to estimate drainage end time by liquid holdup in pipe-time relation curves.

As the only vent point, flow variations at the vent may reveal the evolution of drainage process visually. When the flow rate at the only vent is 0 $m^3/s$ or nearly 0 $m^3/s$ and has no change for a long time till the simulation ends, the drainage can be finished.

Flow rate at the vent-time relation curves of different leaking apertures are given in Fig. 12.

As revealed in Fig. 12, the fluctuation range of the flow rate increases significantly as the leaking aperture gets greater. At the beginning of the leaking, massive water flows through the vent and the liquid hold-up in the branch declines fast, which cause the flow rate at the vent boosts at first and then decreases. Since after water flows through the low elbow, there will be hydrops formed in the low elbow and the residual kinetic energy of the hydrops causes that part of the hydrops effuses from the low elbow, therefore, there is pulsation in flow variation which is illustrated in Fig. 11 that flow rate decreases in the fluctuation and peak showing after a stable value.

But no matter with which leaking aperture, when the drainage proceeds to a certain point in time, there will be no fluctuations in the flow and the order of magnitude of flow rate keeps being $10^{-8}$ until the simulation time is over. This indicates that the flow at the vent has been settled and the drainage process has reached a stabled point (the corresponding settling time is given in Table 4). As shown in Table 4 and Fig. 12, the settling time of flow rate declines first and then increases a bit with the increase of leaking aperture. That is because the greater the aperture is, the more residual kinetic energy the hydrops in the low elbow has, which means more time is needed for the amount of the hydrops to be settled down.

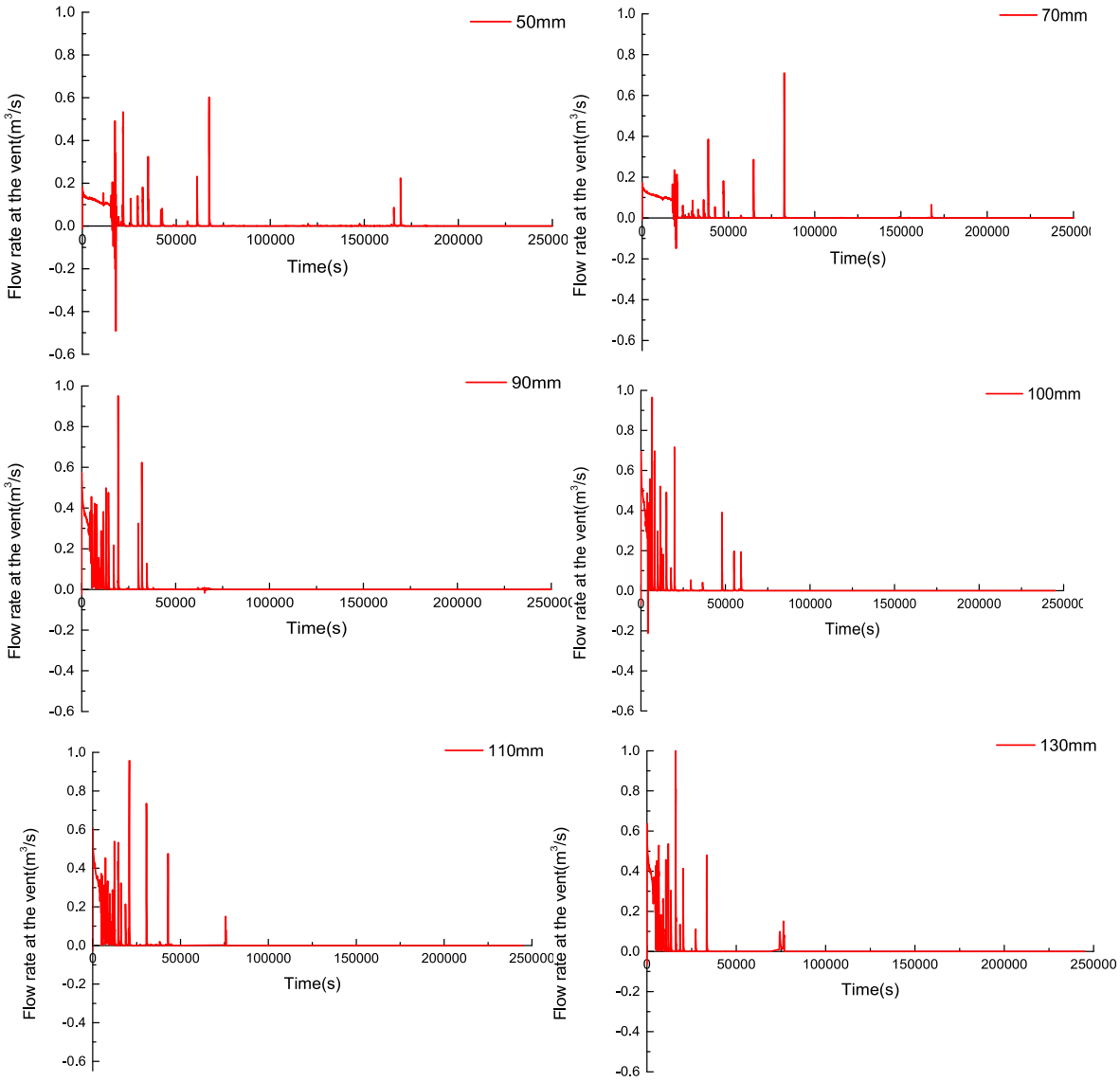


**Fig. 12.** Flow rate at the vent-time relation curves.

### 4.3. Pressure monitoring of key positions

#### 4.3.1. Bottom point

Due to the hilly terrain and big drop of which the maximum relative elevation difference is 460.36 m, the range of pressure fluctuation during the entire drainage process must kept lower than the design pressure of the pipe, 15 MPa, to avoid water hammer and burst in the discharged pipe section. A pressure monitoring site has been set at the bottom point of the pipe to surveil the whole drainage process, and the location of the bottom point site is shown in Fig. 5.

From Fig. 13, the initial pressure at bottom point, which is also the maximum during the whole process, decreases as the vent diameter increases and the greatest one occurs when the vent diameter is 100 mm, which is 4.5 MPa and less than the design pressure of the pipe, 15 MPa. Additionally, there is a trend performed for every available aperture that the pressure at the bottom point reduces sharply from the beginning of discharge, then, fluctuates in a small range, and the pressure variation at the bottom point tends to be steady over time.

#### 4.3.2. Top elbows

Four pressure monitoring sites at the top elbows are set up to in case of negative pressure as these positions usually have low pressure. Taking the situation when the vent diameter is 100 mm as an example, the pressure at the top elbows variation curves are given in Fig. 14.

As demonstrated in Fig. 14, except for top elbow#4, the pressure variation tendencies at other top elbows show basic consistency that pressure drops rapidly from the beginning of drainage then reduces gradually and wavily and eventually fluctuates around a certain value slightly. In terms of top elbow#4, after the sharp drop at the very beginning, the pressure tends to rise smoothly then stays in a constant value with no fluctuation. The pressure at top elbow#1 is the lowest, after 25 200 s, the pressure is often less than 0 Pa, which illustrates that negative pressure situation appears at the top elbows during the drainage, at this time, the pressure at the top elbow#1 is equal to or less than the saturated vapor pressure of water which causes a small amount of water vaporized.

Given the parallel and declining trends of top elbow#1, #2 and #3 and the fact that the minimum pressure appears at the

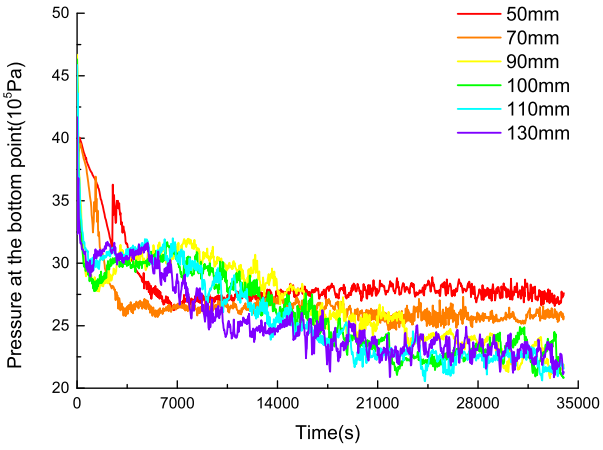


**Fig. 13.** Pressure at the bottom point variation curves.

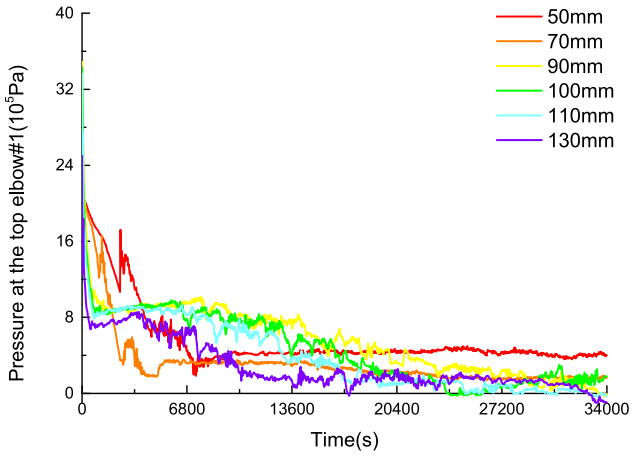


**Fig. 15.** Pressure variation at top elbow#1.

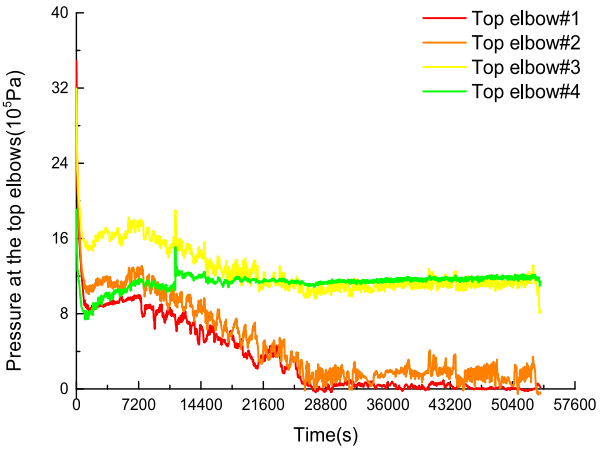


**Fig. 14.** Pressure at top elbow variation curves.

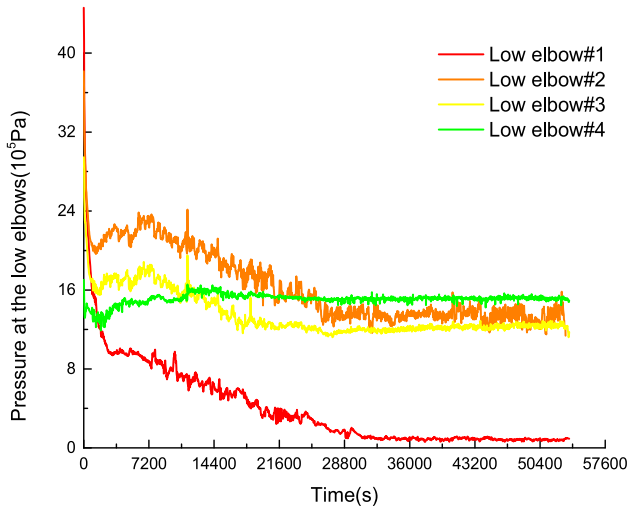


**Fig. 16.** Pressure variation curves at low elbows.

top elbow#1, a comparison among different vent apertures is given in Fig. 15 which demonstrates the relationship between leaking aperture and pressure variation at top elbow by taking top elbow#1 as example.

As shown in Fig. 15, when the leaking aperture is less than 90 mm, the pressure at top elbows responses quite slowly over time; when the aperture is greater than 90 mm, the response over time is obviously accelerated, and the larger the aperture is, the more intense the pressure fluctuation will be, the lower the pressure at the top elbows leads to the deeper degree of negative pressure. However, severe negative pressure fosters the likelihood of close water-surge which will eventually cause damage to the pipe. Consequently, the leaking aperture should not be too large to avoid close water-surge. By the comparison between Figs. 14 and 15, it is found that the general pressure variation trend at top elbows is basically consistent with the one at bottom point, of which the pressure change is merely more intensive.

*4.3.3. Low elbows*

After the water climbs through a top elbow and rushes to the low elbow next to the top one, extra attention is needed to be paid to the pressure variation at the low elbow, for there is a great increase in kinetic energy of water and thus a larger impact will be acted on the pipe wall, which is subjected to the big height difference and has a chance to give rise to water hammer and burst.

Therefore, four pressure monitoring sites are set up at four different low elbows except from the bottom point and their locations are given in Fig. 5.

Pressure variation curves at low elbows are illustrated in Fig. 16 by taking the case when vent diameter is 100 mm as an example.

As shown in Fig. 16, the pressures at the low elbows perform parallel general variation trend as the ones at the top elbows, and the range of pressure changes is from 0.0136 MPa∼4.1 MPa, which is within allowance.

*4.3.4. The vent*

The pressure at the vent variation curves are given in Fig. 17.

In Fig. 17, it seems the general pressure variation tendency at the vent has nothing to do with vent diameters. The pressure drops to a certain value rapidly, then it decreases to a settling value gradually and eventually fluctuates around that settling value slightly. However, the range of fluctuation gets wider and

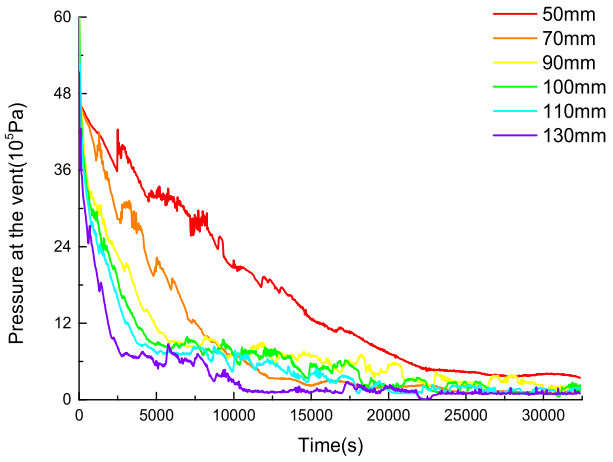


**Fig. 17.** Pressure at the vent-time relation curves.

the settling value of pressure at the vent gets larger with a smaller vent diameter.

## 5. Conclusion

Gas-liquid flow in gas-cap emptying process of a big drop and hilly oil pipeline was numerically investigated based on OLGA7.0 and the simulation results can be concluded as following:

(1) A research of gas-cap emptying process in commissioning of oil pipeline based on OLGA can obtain the flow rate and pressure change trends at the vent, bottom point, top and low elbows, which provides the access to the variation of processing parameters along the entire featured pipeline during the drainage.

(2) As for the emptying of a big drop and hilly pipeline, appropriate increase of leaking aperture can improve the drainage ratio (leakage/general capacity of the pipeline) and drainage rate, but excessive aperture will cause severe negative pressure and breakage cavity which foster the likelihood of close water-surge and damage to the pipe safety.

(3) The general pressure variation tendencies at the vent, bottom point or top and low elbows show no connection with vent diameters but its final fluctuation that the smaller the diameter is, the more intensive the fluctuation gets.

(4) According to the research, the drainage ratio is the highest when the leaking aperture ranges from 90 mm to 110 mm of which the leakage ranges from 3320 $m^3$∼3375 $m^3$ and the settling time of flow rate at the vent is similar but smaller than that of other apertures outside the range, meanwhile, the pressure in the branch is all within allowance during the emptying process, which illustrates that the process is safe. Hence the best leaking aperture range for the pipeline featured in this work is 90 mm∼110 mm based on the analysis above.

**Nomenclature**

$\beta$ = volume fraction
$\rho$ = density
$u$ = velocity
A = pipe cross-sectional area
$\psi_g$ = mass transfer between gas and liquid phases
$\psi_e$ = entrainment rate
$\psi_d$ = deposition rate
$q$ = mass source of phase
$R_D$ = distribution slip ratio caused by an uneven distribution of phases and velocities across the pipe cross sections
$u_r$ = relative velocity
$\theta$ = pipe inclination with horizontal
$u_{0D}$ = falling velocity of droplets
$C_d$ = settling resistance coefficient of droplets
$R_e$ = Reynolds number
$k$ = general heat transfer coefficient of pipeline
$S$ = wetted perimeter
$G$ = mass of phase
$E$ = energy per unit mass
$h$ = elevation
$H$ = enthalpy from mass source
$U$ = transfer from pipe walls

**Subscripts and Superscripts**

$g$ = gas phase
$l$ = liquid
$d$ = liquid droplet
$i$ = interface

## Acknowledgment

This work was supported by the Sichuan Provincial Applied Basic Research Project (2019YJ0352)

## Declaration of competing interest

The authors declare that they have no known competing financial interests or personal relationships that could have appeared to influence the work reported in this paper.

## References

Bonizzi, M., Issa, R.I., 2003. A model for simulating gas bubble entrainment in two-phase horizontal slug flow. Int. J. Multiph. Flow. 29, 1685–1717.
Chao, F., Wang, B., Wu, P., et al., 2016. Analysis of virtual mass force and interfacial pressure on the well-posedness of the two-fluid six-equation model. In: 8th International Symposium on Symbiotic Nuclear Power Systems for 21st Century.
El-Oun, Z., 1990. Gas-Liquid Two-Phase Flow in Pipelines. Society of Petroleum Engineers.
Emonot, P., Souyri, A., Gandrille, J.L., et al., 2011. CATHARE-3: a new system code for thermal-hydraulics in the context of the NEPTUNE project. Nucl. Eng. Des. 241, 4476–4481.
Furfaro, D., Saurel, R., 2015. A simple HLLC-type Riemann solver for compressible non-equilibrium two-phase flows. Comput. & Fluids 111, 159–178.
Guo, B., Song, S., Ghalambor, A., et al., 2014. Gas-liquid multiphase flow in pipeline – Appendix A. In: Offshore Pipelines, second ed. pp. 339–366.
Hongfang, Lu, Kun, Huang, Mohammadamin, Azimi, Lijun, Guo, 2019. Blockchain technology in the oil and gas industry: A review of applications, opportunities, challenges, and risks. IEEE Access 99, 1.
Ishii, M., Mishima, K., 1984. Two-fluid model and hydrodynamic constitutive relations. Nucl. Eng. Des. 82, 107–126.
Issa, R.I., Kempf, M.H.W., 2003. Simulation of slug flow in horizontal and nearly horizontal pipes with the two-fluid model. Int. J. Multiph. Flow. 29, 69–95.
Laanearu, J., Annus, I., Koppel, T., Bergant, A., Vuckovic, S., Hou, Q., Tijsseling, A., Anderson, A., Van't Westende, J., 2012. Emptying of large-scale pipeline by pressurized air. J. Hydraul. Eng. 138 (12), 1090–1100.
Liu, E., Li, W., Cai, H., et al., 2019a. Formation mechanism of trailing oil in product oil pipeline. Processes 7 (1), 7.
Liu, E., Lv, L., Ma, Q., Kuang, J., Zhang, L., 2019b. Steady-state optimization operation of the west-east gas pipeline. Adv. Mech. Eng. 11, 1–14.
Liu, E., Wen, D., Peng, S., et al., 2017. A study of the numerical simulation of water hammer with column separation and cavity collapse in pipelines. Adv. Mech. Eng. 9, 1–13.
Liu, E.B., Yan, S.K., Peng, S.B., 2016. Noise silencing technology for manifold flow noise based on ANSYS fluent. J. Nat. Gas Sci. Eng. 29 (2), 322–328.
Loilier, P., Omgba-Essama, C., Thompson, C., 2005. Numerical experiments of two-phase flow in pipelines with a two-fluid compressible model. In: 12th International Conference on Multiphase Production Technology. Barcelona, Spain.

Lu, L., Zhang, X.H., Lu, X.B., 2017. Numerical study on the stratum's responses due to natural gas hydrate dissociation. Ships Offshore Struct. 12 (6).
Masella, J.M., Tran, Q.H., Ferre, D., et al., 1998. Transient simulation of two-phase flows in pipes. Int. J. Multiph. Flow. 24, 739–755.
Mohammadzaheri, M., et al., 2019. Modelling of petroleum multiphase flow in electrical submersible pumps with shallow artificial neural networks. Ships Offshore Struct..
OLGA, 2014. Dynamic multiphase flow simulator. User's Manual Version 2014.2. Schlumberger.
Omgba-Essama, C., 2004. Numerical Modeling of Transient Gas-Liquid Flow (Application to Stratified and Slug Flows) (Ph.D. thesis). AMAC, Canfield University, UK.
Pouraria, H., et al., 2017. Numerical study of erosion in critical components of subsea pipeline: tees vs bends. Ships Offshore Struct. 12 (2).
Saurel, R., Abgrall, R., 1999. A Multiphase Godunov Method for Compressible Multi-Fluid and Multiphase Flows. Academic Press Professional, Inc.
Seung, Jun Lee, Jae, Hwa Lee, Byoung, Jae Kim, 2017. Improvement of the two-fluid momentum equation using a modified reynolds stress model for horizontal turbulent bubbly flows. Chem. Eng. Sci. 173, 208–217.
Shanbi, Peng, Wen, Liao, Huan, Tan, 2018. Performance optimization of ultrasonic flow meter based on computational fluid dynamics. Adv. Mech. Eng. 10, 1–9.
Shanfang, Huang, Bingdong, Zhang, Jun, Lu, et al., 2013. Study on flow pattern maps in hilly-terrain air–water–oil three-phase flows. Exp. Therm Fluid Sci. 47, 158–171.
Simões, E.F, Carneiro, J.N.E., Nieckele, A.O., 2014. Numerical prediction of non-boiling heat transfer in horizontal stratified and slug flow by two-fluid model. Int. J. Heat Fluid Flow 47, 134–145.
Taitel, Y., et al., 1995. Stratified three phase flow in pipelines. Int. J. Multiph. Flow. 3, 53–60.
Tijsseling, A., Hou, Q., Bozkus, Z., Laanearu, J., 2016. Improved one-dimensional models for rapid emptying and filling of pipelines. J. Press. Vessel Technol. 138 (3).
Yacin, Salhi, El-khider, Si-Ahmed, et al., 2010. Stability analysis of inclined stratified two-phase gas–liquid flow. Nucl. Eng. Des. 240, 1083–1096.
Yeoh, G.H., Tu, J., 2010. Gas-liquid flows. Comput. Tech. Multip. Flows 135–456.